

Zero-bias conductance in carbon nanotube quantum dots

Frithjof B. Anders,¹ David E. Logan,² Martin R. Galpin,² and Gleb Finkelstein³

¹*Institut für Theoretische Physik, Universität Bremen, P.O. Box 330 440, D-28334 Bremen, Germany*

²*Physical and Theoretical Chemistry, Oxford University, South Parks Road, Oxford OX1 3QZ, UK*

³*Department of Physics, Duke University, Durham, North Carolina 27708, USA*

(Dated: February 6, 2020)

We present numerical renormalization group calculations for the zero-bias conductance of quantum dots made from semiconducting carbon nanotubes. These explain and reproduce the thermal evolution of the conductance for different groups of orbitals, as the dot-lead tunnel coupling is varied and the system evolves from correlated Kondo behavior to more weakly correlated regimes. For integer fillings $N = 1, 2, 3$ of an $SU(4)$ model, we find universal scaling behavior of the conductance that is distinct from the standard $SU(2)$ universal conductance, and concurs quantitatively with experiment. Our results also agree qualitatively with experimental differential conductance maps.

Introduction: Carbon nanotubes have generated immense interest due to their rich transport properties [1]. Their small capacitance generates a Coulomb blockade regime at low temperatures [2], and a single electron transistor [2, 3] can be made out of weakly coupled nanotubes. The Kondo effect, studied in transition metal ions and rare earth compounds for some fifty years [4, 5], is now equally a classic hallmark of many-body physics in nanoscale devices, including carbon nanotubes [6] as well as semiconducting quantum dots, molecules and magnetic adatoms on metallic surfaces (for a review see [7]).

While the ‘standard’ Kondo effect arising in nano-devices is the orbitally non-degenerate, spin- $\frac{1}{2}$ ($SU(2)$) Kondo effect [4], it is known that in quantum dots made from high quality nanotubes, a series of *two* spin-degenerate orbitals originates from the two electronic sub-bands [8, 9]. Consecutive filling of these orbitals should thus yield an $SU(4)$ -type Kondo effect [4, 10, 11, 12, 13, 14, 15, 16, 17, 18, 19, 20]. This has indeed been observed in recent experiments [10, 11, 12], including in particular systematic exploration of the $SU(4)$ conductance regimes [12] via careful control of sample contact transparency.

In this paper, we present a consistent picture which explains the experimental zero bias conductance [12]. We study the thermal evolution of the conductance as a function of applied gate voltage, for an $SU(4)$ Anderson model, using Wilson’s numerical renormalization group (NRG) [5, 21]; and show that on progressive increase of the dot-lead tunnel couplings, the system exhibits a rich evolution from correlated Kondo behavior with strong associated Coulomb blockade peaks in the zero-bias conductance, through to a weaker coupling regime where charge fluctuations are significant and Coulomb blockade oscillations suppressed. We obtain universal scaling functions for the zero-bias conductance, which deviate significantly from standard $SU(2)$ Kondo scaling (reflecting the different universality class of our model); and show that this captures experiment quantitatively.

Theory: Interacting quantum dots, molecular junctions and other nano-devices are modelled by the in-

teracting region \mathcal{H}_{imp} , a set of non-interacting reservoirs \mathcal{H}_B and a coupling between the subsystems \mathcal{H}_T : $\mathcal{H} = \mathcal{H}_{imp} + \mathcal{H}_B + \mathcal{H}_T$. For the carbon nanotube quantum dot we restrict ourselves to the filling of one shell comprising two degenerate orbitals, and consider the local Hamiltonian $\mathcal{H}_{imp} = \frac{1}{2}U(\hat{N} - N_g)^2$. Here $\hat{N} = \sum_{\alpha\sigma} d_{\alpha\sigma}^\dagger d_{\alpha\sigma} = \sum_{\alpha\sigma} \hat{n}_{\alpha\sigma}$, where $d_{\sigma\alpha}^\dagger$ creates a σ -spin electron in orbital $\alpha = 1, 2$, the charging energy $U = e^2/C \equiv E_C$ with dot capacitance C , and N_g denotes the dimensionless external gate voltage. Equivalently,

$$\mathcal{H}_{imp} = E_d \hat{N} + \frac{1}{2}U \sum_{m,m'(m' \neq m)} \hat{n}_m \hat{n}_{m'} \quad (1)$$

with level energy $E_d = \frac{U}{2}(1 - 2N_g)$ and $m \equiv (\alpha, \sigma)$ a flavor index. For the isolated dot, with integer ground state charge $N_d = 0 - 4$, the edges in the Coulomb blockade staircase between charge N_d and $N_d + 1$ occur for half-integer $N_g = \frac{1}{2}(2N_d + 1)$ (ie $E_d = -UN_d$). In Eq.(1) we have taken $U' = U$, with U [U'] the intra- [inter-] orbital Coulomb repulsion, and have also neglected an exchange splitting, J . This is consistent with the argument [22] that for carbon nanotubes, $U' \simeq U$ and J is much smaller than the charge fluctuation scale; and is known to be compatible with the carbon nanotube data [23].

The tunneling to the two leads $\nu = L, R$ is assumed to be spin and orbital conserving [12, 18],

$$\mathcal{H}_T = \sum_{\alpha,\nu} \tilde{t}_\nu \sum_{k,\sigma} \left(c_{k\sigma\alpha\nu}^\dagger d_{\sigma\alpha} + d_{\sigma\alpha}^\dagger c_{k\sigma\alpha\nu} \right) \quad (2)$$

such that the overall \mathcal{H} has $SU(4)$ symmetry. Only the binding combination of lead states, $c_{k\sigma\alpha} = \frac{1}{t} \sum_\nu \tilde{t}_\nu c_{k\sigma\alpha\nu}$ with $t = [\tilde{t}_L^2 + \tilde{t}_R^2]^{\frac{1}{2}}$, then couples to the dot. We can thus drop the lead index ν and consider one effective lead:

$$\mathcal{H}_B = \sum_{k\sigma\alpha} \epsilon_k c_{k\sigma\alpha}^\dagger c_{k\sigma\alpha} \cdot \quad (3)$$

Note however that the different coupling strengths still enter through the conductance prefactor $G_0 = (e^2/h)4\Gamma_L\Gamma_R/(\Gamma_L+\Gamma_R)^2$, which reaches the unitary limit

of e^2/h for a perfect symmetric channel $\Gamma_L = \Gamma_R$ [24], where $\Gamma_\nu = \pi \tilde{t}_\nu^2 \rho$ with ρ the density of states of the leads at the Fermi energy.

Method: We solve the Hamiltonian accurately using the NRG approach [5, 21]. The key ingredient in NRG is a logarithmic discretization of the continuous bath/lead, controlled by the parameter $\Lambda > 1$. The Hamiltonian is mapped onto a semi-infinite chain, where the N th link represents an exponentially decreasing energy scale $D_N \sim \Lambda^{-N/2}$ (with D the lead bandwidth). Using this hierarchy of scales the sequence of finite-size Hamiltonians \mathcal{H}_N for the N -site chain is solved iteratively, discarding the high-energy states at each step to maintain a manageable number (N_s) of states. This reduced basis set of \mathcal{H}_N faithfully describes the spectrum of the full Hamiltonian on the scale of D_N , corresponding [5] to a temperature $T_N \sim D_N$ from which all thermodynamic expectation values are calculated. For further details we refer to the recent review [21].

Finite temperature NRG Green's functions are calculated using the recently developed algorithm [25, 26], employing a complete basis set of the Wilson chain. Originally derived for real-time dynamics of quantum impurities out of equilibrium [27, 28], this ensures that the spectral sum-rule is exactly fulfilled and the NRG occupancy accurately reproduced. The self-energy of the Green function is calculated in the usual way [29].

The local Green function determining transport is given by $G_\alpha^d(z) = [z - \epsilon - \Delta(z) - \Sigma(z)]^{-1}$ with $z = \omega + i0^-$, $\Delta = \sum_\nu \tilde{t}_\nu^2 \sum_k [z - \epsilon_k]^{-1}$ the dot-lead hybridization, and $\Sigma(z)$ the interaction self-energy; the local spectrum is $D(\omega, T) = \frac{1}{\pi} \Im m G_\alpha^d(z)$. At $T = 0$, the Friedel sum rule [30, 31] relates the number of impurity electrons N_{imp} to the conduction electron scattering phase shift $\delta = \pi N_{imp}/N$, where N is the number of channels (here $N = 4$). $N_{imp} = N_d + \Delta N$ includes all electrons on the quantum dot ($N_d = \langle \sum_{\alpha,\sigma} \hat{n}_{\alpha\sigma} \rangle$) and the number of displaced electrons in the bath ΔN [31], and can be obtained directly from the NRG [5]. For a vanishing $\Im m \Sigma_{\sigma\alpha}(i0^-)$ as $T \rightarrow 0$, the zero bias conductance must approach

$$\lim_{T \rightarrow 0} G(T) = 4G_0 \sin^2(\delta) = 4G_0 \sin^2\left(\frac{\pi}{4} N_{imp}\right) \quad (4)$$

which is indeed recovered in our calculations.

Results: We use a symmetric, constant lead density of states $\rho_0 = 1/(2D)$ with a band width $D = 30\Gamma_0$, $\Gamma_0 = 1meV \simeq 11.6K$ being the energy unit used throughout. We take $U = 10\Gamma_0 = 10meV$, corresponding to the experimental estimate of the charging energy $E_C \equiv U$ [12].

One of the striking, poorly understood features of the recent experiments on semiconducting carbon nanotube dots [12] is the thermal evolution of the zero bias conductance as a function of gate voltage. In the experiment, the orbitals are filled in groups of two (there being four such groups, I-IV [12]). In addition, the tunneling matrix elements increase with gate voltage. We restrict ourselves

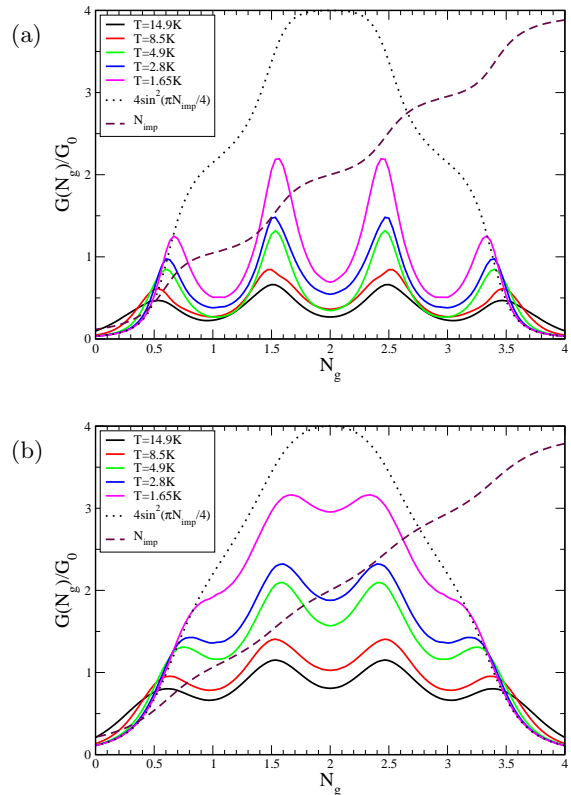


FIG. 1: (color online) Zero bias conductance *vs* dimensionless gate voltage N_g , for different T and two tunneling strengths $\Gamma = 0.5meV$ ((a)), $1meV$ ((b)); with $U \equiv E_C = 10meV$. The dotted line gives the $T = 0$ values, Eq. (4); N_{imp} is also shown (dashed line). NRG parameters: $\Lambda = 3$, $N_s = 2000$.

to a single representative group, keeping the tunneling matrix elements constant for simplicity; and calculate the zero-bias conductance as a function of the dimensionless gate voltage N_g , for different tunneling strengths $\Gamma = \Gamma_L + \Gamma_R$ and temperatures, using the NRG spectral functions: $G(T)/G_0 = -4 \int_{-\infty}^{\infty} d\omega (\partial f(\omega)/\partial \omega) t(\omega)$ with $t(\omega) = \pi \Gamma D(\omega)$ the t -matrix and $f(\omega)$ the Fermi function. The results are given in Figs. 1 and 2 for three different coupling strengths $\Gamma = 0.5\Gamma_0, \Gamma_0, 2\Gamma_0$.

Our results concur well with experiment. Those for $\Gamma = 0.5meV$ (Fig. 1a) track the T -evolution of Group I depicted in Fig. 2 of Ref. [12]. Clear, pronounced Coulomb blockade peaks and valleys are seen in Fig. 1a. These disappear only at temperatures much lower than the experimental base $T = 1.3K$, indicative of strong correlations ($U/\Gamma = 20$ here) and hence small Kondo scales T_K in the middle of the valleys ($N_g = 1$ (3) and 2). The distance between the peaks is seen to become smaller with decreasing T , also in agreement with experiment. The origin is a pinning of the many-body Kondo resonance in $D(\omega)$ close to the chemical potential at low- T , evident in the t -matrix depicted in Fig. 5 (discussed below). For $T = 0$, the conductance from the Friedel sum

rule Eq. (4) is shown as a dotted line in Fig. 1a. Absolute values of $G(T)$ also agree well with experiment. For Group I [12] the coupling asymmetry is $\Gamma_L/\Gamma_R \approx 2.5$, and hence $G_0 \simeq 0.8e^2/h$. With this, *eg* the calculated $N_g = 1.5$ (or 2.5) Coulomb blockade peak in $G(T)$ for $T = 1.65K$ translates to $G_{peak} \approx 1.7e^2/h$, in good agreement with experiment; and the widths of the peaks also concur with experiment. The slight experimental asymmetry of the $N_g = 0.5$ and 3.5 Group I conductance peaks can be attributed to a small increase in the tunnel coupling within the Group on increasing the gate voltage.

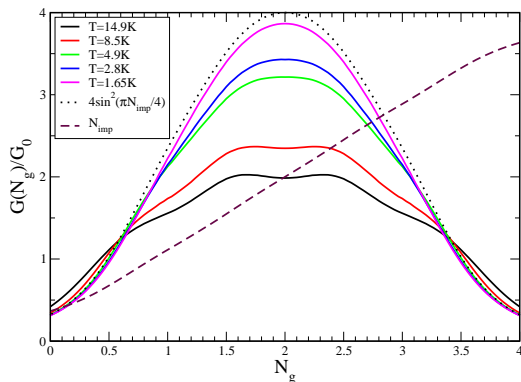


FIG. 2: (color online) Zero bias conductance vs N_g for different temperatures and $\Gamma = 2meV$. The dotted line gives the $T = 0$ values from Eq. (4). Other parameters as in Fig. 1.

Results for $\Gamma = 1meV$ ($U/\Gamma = 10$, Fig. 1b) resemble the experimental Group III orbitals [12]. At higher T , remnants of the Coulomb blockade peaks remain visible; they are absent at base temperature. While for stronger correlations (*eg* Fig. 1a) the charge steps are quite pronounced, and the different orbital filling regimes well separated in the $T = 0$ conductance, for $U/\Gamma = 10$ orbital filling is almost continuous. The physical origin of such behavior is in part the ‘blocking effect’ known from the theory of multi-channel models in the context of rare earth materials [13], in which Coulomb interactions lead to single-particle lifetime broadening of order $N\Gamma$, since N relaxation channels are present. In addition, the $SU(4)$ Kondo scale in the Kondo regime is much larger than for $SU(2)$ as the number of channels enters the exponent, $T_K^{SU(4)}/D \simeq [T_K^{SU(2)}/D]^{1/2}$ [4, 16]. In consequence, an $SU(4)$ model enters the weakly correlated regime for larger U/Γ than an $SU(2)$ symmetric model.

Fig. 2 shows results for a more weakly correlated $U/\Gamma = 5$. This tracks the T -evolution of the Group IV orbitals [12]. Here, consistent with experiment, charge fluctuations are significant and Coulomb blockade peaks in consequence absent, with the $G(T \rightarrow 0)$ limit Eqn. (4) being reached in practice at relatively high temperatures.

The T -dependence of $G(T)$ for the middle of the Coulomb valleys, $N_g = 2$ and $N_g = 1$ (or 3), is shown in Fig. 3 for five values of Γ . Comparison of the two shows

the characteristic energy scales in all valleys are of the same order (see also Fig. 4 inset): the Coulomb blockade valleys are thus filled simultaneously with decreasing T , as seen in experiment [12]. This in turn provides strong evidence for $U' = U$, since only a very slight decrease of U' from the $SU(4)$ point $U' = U$ causes a sharp drop in the $N_g = 2$ Kondo scale towards $SU(2)$ form [16], while the $N_g = 1$ scale is by contrast barely affected [16, 19].

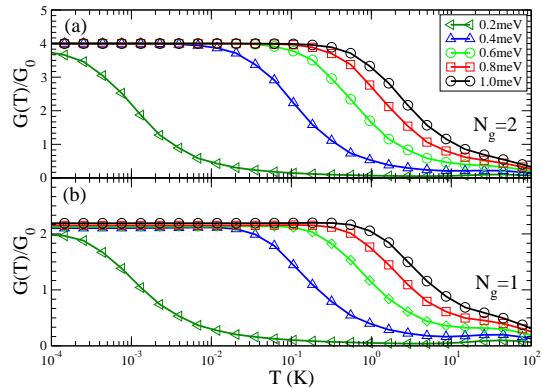


FIG. 3: (color online) T -dependence of $G(T)$ for five different values of Γ and two different dimensionless gate voltages: (a) $N_g = 2$ and (b) $N_g = 1$ (or $N_g = 3$).

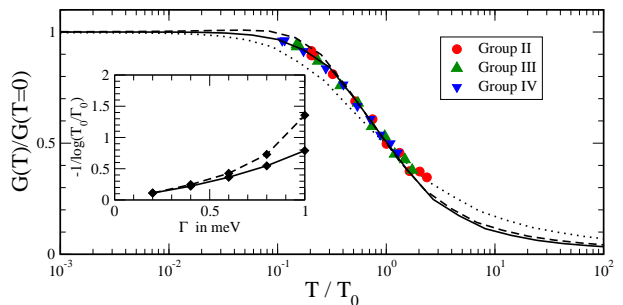


FIG. 4: (color online) $SU(4)$ scaling conductance $g(x) = G(T)/G(0)$ vs $x = T/T_0$ – solid line for $N_g = 2$, dashed for $N_g = 1$ (or 3). The $SU(2)$ scaling conductance is shown as a dotted line. Experimental results [12] for Groups II, III and IV (with $N_g = 2$) are also shown. Inset: evolution of the low-energy scale T_0 , for $N_g = 2$ (solid) and $N_g = 1$ (dashed).

Defining a characteristic low-energy scale T_0 ($\propto T_K$) by $G(T_0)/G(0) = 0.5$, yields scaling collapse onto universal $SU(4)$ conductance curves $g(x) = G(T)/G(0)$ vs $x = T/T_0$, as shown in Fig. 4. For $x \gtrsim 1$, $g(x)$ for $N_g = 2$ and 1 asymptotically coincide, while for lower x the two are distinct (reflecting different leading corrections to the $SU(4)$ fixed point). The corresponding universal conductance for a symmetric $SU(2)$ model is also shown. It is seen to have a quite different form, and is known [12] not to fit well the carbon nanotube data. For the $SU(4)$ model by contrast, the results of our theory agree well with experiment – as seen in Fig. 4 where experimental

results for Groups II, III and IV in the middle of the two-electron valleys [12] are compared to the $N_g = 2$ $SU(4)$ scaling conductance. At sufficiently high T , departure from universal scaling must inevitably occur (as just visible for the Group II, III data), but the data collapse remarkably well onto the scaling conductance [32].

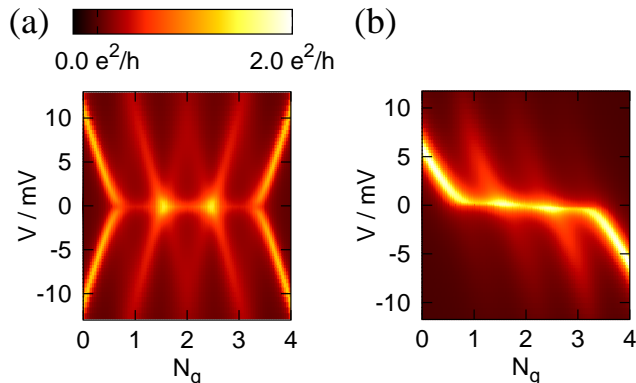


FIG. 5: (color online) Color-coded contour plot in the (V, N_g) -plane of (a) $t_s(V, N_g)$ for $\Gamma = 0.5 \text{ meV}$ at $T = 2.8 \text{ K}$, as in Fig. 1a; (b) $t(\omega = eV)$ for $\Gamma = 1 \text{ meV}$ as in Fig. 1b.

Finally, to assess approximately the effects of a finite source-drain bias $V_{sd} \equiv V$, we neglect explicit dependence of the self-energy on V . Granted this, if one of the contacts is sufficiently open that it acts as a tunneling probe, the $T = 0$ conductance $G(V, N_g) \propto t(\omega = eV)$ with $t(\omega)$ the t -matrix as above. This situation is appropriate to the Group III and IV orbitals of [12]. If by contrast the contacts are more symmetrically coupled, then $G(V, N_g) \propto t_s(V, N_g) = \frac{1}{2}[t(\omega = +\frac{1}{2}eV) + t(\omega = -\frac{1}{2}eV)]$ [24]. This we believe is the relevant case for the Group I orbitals of [12]. For $\Gamma = 0.5 \text{ meV}$ (as in Fig. 1a), Fig. 5a shows a contour plot of $G_0 t_s(V, N_g)$ (calculated for $T = 2.8 \text{ K}$ [33]). The striking similarity to the experimental Group I differential conductance map (Fig. 2b of [12]) is evident, including the clear Coulomb blockade diamonds. For $\Gamma = 1 \text{ meV}$ (as in Fig. 1b), Fig. 5b shows a corresponding contour plot of $G_0 t(\omega = eV)$; this in turn captures well the Group III conductance map [12].

Conclusion: Motivated by recent experiments on carbon nanotube quantum dots [12], we have studied the evolution of an $SU(4)$ Anderson model from correlated Kondo to mixed valent behavior, on progressive increase of the dot-lead tunnel couplings. NRG results obtained are in compelling agreement with experiment [12], from the thermal evolution and scaling behavior of the zero-bias conductance, to differential conductance maps; and show that an $SU(4)$ Anderson model provides a remarkably faithful description of carbon nanotube dots.

We acknowledge stimulating discussions with A. Schiller. This research was supported in part by DFG project AN 275/5-1 and NSF Grant No.

PHY05-51164 (FBA), by EPSRC Grant EP/D050952/1 (DEL/MRG) and by NSF Grant DMR-0239748 (GF). We acknowledge supercomputer support by the NIC, Forschungszentrum Jülich under project No. HHB000.

-
- [1] C. Dekker, *Phys. Today* **52**, 22 (1999).
 - [2] S. J. Tans et al., *Nature* **386**, 474 (1997).
 - [3] M. A. Kastner, *Rev. Mod. Phys.* **64**, 849 (1992).
 - [4] A. C. Hewson, *The Kondo Problem to Heavy Fermions* (Cambridge Press, Cambridge UK, 1993).
 - [5] K. G. Wilson, *Rev. Mod. Phys.* **47**, 773 (1975).
 - [6] J. Nygard, D. Cobden, and P. Lindelhof, *Nature* **408**, 342 (2000).
 - [7] L. P. Kouwenhoven and L. I. Glazman, *Phys. World* **14**, 33 (2001).
 - [8] W. J. Liang, M. Bockrath, and H. Park, *Phys. Rev. Lett.* **88**, 126801 (2002).
 - [9] M. R. Buitelaar et al., *Phys. Rev. Lett.* **88**, 156801 (2002).
 - [10] P. Jarillo-Herrero et al., *Nature* **434**, 484 (2005).
 - [11] A. Makarovski, J. Liu, and G. Finkelstein, *Phys. Rev. B* **75**, 241407 (2007).
 - [12] A. Makarovski, A. Zhukov, J. Liu, and G. Finkelstein, *Phys. Rev. Lett.* **99**, 066801 (2007).
 - [13] N. E. Bickers, *Rev. Mod. Phys.* **59**, 845 (1987).
 - [14] D. Boese, W. Hofstetter, and H. Schoeller, *Phys. Rev. B* **66**, 125315 (2002).
 - [15] L. Borda et al., *Phys. Rev. Lett.* **90**, 026602 (2003).
 - [16] M. R. Galpin, D. E. Logan, and H. R. Krishnamurthy, *Phys. Rev. Lett.* **94**, 186406 (2005).
 - [17] R. Lopez et al., *Phys. Rev. B* **71**, 115312 (2005).
 - [18] M. S. Choi, R. Lopez, and R. Aguado, *Phys. Rev. Lett.* **95**, 067294 (2005).
 - [19] A. K. Mitchell, M. R. Galpin, and D. E. Logan, *Europhys. Lett.* **76**, 95 (2006).
 - [20] C. A. Büsser and G. B. Martins, *Phys. Rev. B* **75**, 045406 (2007).
 - [21] R. Bulla, T. Costi, and T. Pruschke, *cond-mat/0701105* (2007).
 - [22] Y. Oreg, K. Byczuk, and B. I. Halperin, *Phys. Rev. Lett.* **85**, 365 (2000).
 - [23] A. Makarovski, L. An, J. Liu, and G. Finkelstein, *Phys. Rev. B* **74**, 155431 (2006).
 - [24] Y. Meir and N. S. Wingreen, *Phys. Rev. Lett.* **68**, 2512 (1992).
 - [25] R. Peters, T. Pruschke, and F. B. Anders, *Phys. Rev. B* **74**, 245114 (2006).
 - [26] A. Weichselbaum and J. von Delft, *Phys. Rev. Lett.* **99**, 076402 (2007).
 - [27] F. B. Anders and A. Schiller, *Phys. Rev. Lett.* **95**, 196801 (2005).
 - [28] F. B. Anders and A. Schiller, *Phys. Rev. B* **74**, 195119 (2006).
 - [29] R. Bulla, A. C. Hewson, and T. Pruschke, *J. Phys.: Condens. Matter* **10**, 8365 (1998).
 - [30] D. C. Langreth, *Phys. Rev.* **150**, 516 (1966).
 - [31] F. B. Anders, N. Grewe, and A. Lorek, *Z. Phys. B Condensed Matter* **83**, 7 (1991).
 - [32] Results for Group I (smallest Γ) lie slightly outside the scaling regime for most of the experimental T -range.

[33] Additional thermal smearing of $G(V, N_g)$ from finite- T

Fermi functions is a minor effect.